

# Efficient and Effective $L_0$ Feature Selection

Ana Kenney<sup>1</sup>, Francesca Chiaromonte<sup>1, 2</sup>, and Giovanni Felici<sup>3</sup>

<sup>1</sup>Dept. of Statistics, Penn State University.

<sup>2</sup>Inst. of Economics & EMBeDS, Sant'Anna School of Advanced Studies.

<sup>3</sup>Istituto di Analisi dei Sistemi ed Informatica, Consiglio Nazionale delle Ricerche.

## Abstract

Because of continuous advances in mathematical programming, Mix Integer Optimization has become a competitive vis-a-vis popular regularization method for selecting features in regression problems. The approach exhibits unquestionable foundational appeal and versatility, but also poses important challenges. We tackle these challenges, reducing computational burden when tuning the sparsity bound (a parameter which is critical for effectiveness) and improving performance in the presence of feature collinearity and of signals that vary in nature and strength. Importantly, we render the approach efficient and effective in applications of realistic size and complexity without resorting to relaxations or heuristics in the optimization, or abandoning rigorous cross-validation tuning. Computational viability and improved performance in subtler scenarios is achieved with a multi-pronged blueprint, leveraging characteristics of the Mixed Integer Programming framework and by means of whitening, a data pre-processing step.

## 1 Introduction

LASSO-type methods (e.g., [Tibshirani, 1996], [Zou and Hastie, 2005], [Meier et al., 2008]) perform feature selection as a convex constrained optimization, shrinking the  $L_1$  norm of the coefficient estimates vector. While inducing sparsity, LASSO does not constrain directly the number of non-zero estimates (the size of the so-called *active set* of features). However, it is enormously popular due to its effectiveness and computational efficiency in comparison to traditional best subset selection, which explores all subsets of any size and is computationally very demanding, or sequential procedures, which curb computation but may lead to suboptimal solutions especially in the presence of collinear features. Recently, a new approach based on Mixed Integer Optimization has been brought to bear onto this statistical problem. By very efficiently tackling integrality constraints, advances in optimization methods allow direct control of the  $L_0$  norm of the coefficient estimates vector (the size of the active set), and thus sparsity, in larger problems (see [Bertsimas et al., 2016] and [Bertsimas et al., 2017] for standard and logistic regression). This, which we refer to as the Mixed Integer Programming (MIP) approach, has engendered a lively debate (e.g., [Hastie et al., 2017], [Mazumder et al., 2017], [Bertsimas and Van Parys, 2017]) comparing its general phylosophy and performance to the LASSO. A notable outcome of this debate has been the proposal of hybrid approaches, whereby the non-zero coefficient estimates of a LASSO solution are allowed to “unshrink” (relaxed LASSO, [Hastie et al., 2017]), or some shrinkage is imposed upon a MIP solution by adding  $L_1$  and/or  $L_2$  norm constraints to the problem (penalized MIP, [Mazumder et al., 2017]).

While LASSO-type methods remain unquestionaly best in terms of computational burden for any problem size, the MIP approach, at least in its existing implementations, is *not* viable for realistic problem sizes (hundreds, thousands or more features) if one seeks to appropriately tune the  $L_0$  constraint which is critical for effectiveness. Moreover, which approach works best in terms of prediction, coefficients estimation and active set identification depends on problem complexity.

When the sample size is relatively modest with respect to the number of features, a trade-off can emerge between model parsimony and the balancing of bias and variance in coefficients estimation. In addition, signal strength and patterns, degree of (true) underlying sparsity, and linear associations among the features can have important effects. To date, performance of the MIP approach in comparison to LASSO-type methods is still only partially understood in the presence feature collinearity and signals that vary in nature and strength. Pondering these issues from the perspective of applications and impact on statistical practice, our aim is to render the MIP approach efficient and effective in applications of realistic size and complexity.

Back to tuning, best practices involve assessing out-of-sample performance, e.g. by cross-validation – notably, this is an integral part of all LASSO implementations. But for a problem comprising  $p$  features, tuning the MIP approach by standard  $v$ -fold cross-validation over the whole range of its main parameter (the sparsity bound, i.e. the size of the active set) requires solving  $v \times p$  optimizations each of which can be itself computationally demanding. Though metrics such as AIC or BIC (Akaike and Bayes Information Criteria) can in principle be used to avoid cross-validation, they rely on distributional assumptions and asymptotic properties. Interestingly, [Miyashiro and Takano, 2015] treat information criteria as the objective in a reformulated MIP which must be solved only once, with the bound value internally determined – but this was found to be in fact slower than solving the original MIP over all possible values of the bound. Proposals also exist to improve the computational efficiency of each individual MIP run, usually adopting sub-optimal solutions based on linear relaxations and heuristics. For instance, [Willis and von Stosch, 2017] use approximations of the  $L_0$  norm and solve the reformulated problem with sequential linear programming, and [Hazimeh and Mazumder, 2018] use a coordinate descent with local combinatorial search to fit a sparse ridge regression – obtaining solutions similar to those of the original MIP. These proposals though do not provide a provable guarantee on solution quality weakening the appeal of the MIP approach.

We believe that computational burden should not discourage the widespread use of MIP for feature selection, nor the quest for efficient techniques to solve the problem at optimality. In fact, in addition to direct control of sparsity, the MIP approach affords several other important advantages. In particular, it allows one to incorporate further constraints and adjust the objective function to enhance desirable problem-specific properties. For instance, [Bertsimas et al., 2017] exploited this in logistic regression to address issues such as group sparsity, multicollinearity among selected features, robustness of solutions, statistical significance, modeler expertise, etc. As another instance, in a classification problem for microarray data, [Lan and Vucetic, 2013] used Binary Integer Programming to select a subset of genes that was not only predictive of class label, but also minimally redundant. Previously, prediction performance and redundancy had been targeted separately by repeatedly refitting and adjusting the model to improve results – but the two objectives can be pursued simultaneously within the MIP framework, as for example in [Felici et al., 2017].

Our proposals do not resort to relaxations or heuristics in the optimization problem, and do not abandon rigorous cross-validation based tuning. We recover computational viability and improve performance in subtler application scenarios with a multi-pronged blueprint that leverages characteristics of the MIP framework. We also explore the use of whitening, a data pre-processing technique to de-correlate features, as a means to increase feature selection accuracy in applications where high collinearity and/or weak signals result in a failure to identify all (or only) relevant features. We find that the MIP approach greatly benefits from whitening and, interestingly, that it exploits this pre-processing step more effectively than LASSO-type methods. In short, in this article we introduce:

1. two **modified bisection procedures**, which allow us to assess the whole range of the MIP

tuning parameter directly evaluating only a small portion of its values;

2. strategies for **bounds and warm starts**, based on the auxiliary use of LASSO and forward selection, which can be called upon to speed up convergence in particularly slow optimization runs;
3. an **integrated cross-validation scheme**, which exploits the nature of mixed integer programs and, in combination with (1) and (2), drastically reduces computation time;
4. **whitening** as a pre-processing step to better handle collinear features and a wide range of signal strengths.

Before describing our proposals in Section 3, we provide some technical background and formulate best subset selection as a MIP problem in Section 2. In Section 4 we present results of an in depth simulation study, and an application to a Diabetes data set first introduced in [Efron et al., 2004]. Concluding remarks are provided in Section 5.

## 2 Background

As background for our work, we briefly describe Mixed Integer Programs in Section 2.1, best subset selection as a Mixed Integer Quadratic Program in Section 2.2, and the typical LASSO approach to feature selection in Section 2.3.

### 2.1 Mixed Integer Programming

In Mixed Integer Programs (MIP), an objective function is optimized under a collection of constraints – including constraints that require some of the variables to assume only integer values (integrality constraints). A well studied and rather general class of MIPs is that of Mixed Integer Quadratic Programs (MIQP), where a quadratic objective function is optimized under both linear and integrality constraints. In symbols

$$\min_{\mathbf{v}} \mathbf{v}^T Q \mathbf{v} + \mathbf{q}^T \mathbf{v} \quad (1a)$$

$$A\mathbf{v} \leq \mathbf{b} \quad (1b)$$

$$\mathbf{l} \leq \mathbf{v} \leq \mathbf{u} \quad (1c)$$

$$v_j \in \mathcal{S} \subset \mathbb{Z} \text{ for } j \in \mathcal{J} \subset \{1, 2, \dots, p\} \quad (1d)$$

where  $\mathbf{v} \in \mathbb{R}^p$  is the vector of variables, and  $\mathbf{q} \in \mathbb{R}^n$ ,  $Q \in \mathbb{R}^{n \times p}$  (positive semidefinite),  $A \in \mathbb{R}^{n \times p}$ ,  $\mathbf{b} \in \mathbb{R}^n$ , and  $\mathbf{l}, \mathbf{u} \in \mathbb{R}^p$  are known quantities. (1b) expresses the linear constraints, (1c) lower and upper bounds on the feasible values of the solution vector, and (1d) the integrality constraints; variables in the index set  $\mathcal{J}$  can take only integer values in the set  $\mathcal{S}$ .

MIQPs are of particular interest to us because regression and its feature selection commonly utilize least squares; that is, a quadratic objective function. They extend an even better studied class of MIPs; Mixed Integer Linear Programs (MILP), where also the objective function is linear. In turn, MILPs extend the simplest class of programs; Linear Programs (LP), where integrality constraints are absent.

From a computational point of view, LPs of any size can be solved very quickly. But introducing integrality constraints, even in the form of binary constraints restricting variables to  $\{0, 1\}$ , poses serious challenges – both in the case of linear objective functions (MILPs) and in the case of quadratic ones (MIQPs). Nevertheless, optimization solvers have seen dramatic improvements in

the past two decades; see [Bertsimas et al., 2016] for an overview of progress from 1991 through 2015. At present, the most effective way to solve a MIP problem is to relax integrality constraints and then combine implicit enumeration methods, such as Branch & Bound, with the addition of constraints that approximate integrality in the relaxed problem, such as Branch & Cut (for a general introduction to these techniques see [Schrijver, 1986]). The overarching goal of recent contributions (see in particular [Bertsimas et al., 2016]) and of our own work, is indeed to harness this extremely powerful machinery for the purpose of feature selection.

## 2.2 Best Subset Selection as a Mixed Integer Quadratic Program

Consider a linear regression of the form  $\mathbf{Y} = \mathbf{X}\boldsymbol{\beta} + \boldsymbol{\epsilon}$ , where  $\mathbf{Y} \in \mathbb{R}^n$  is the vector of response values,  $\mathbf{X} \in \mathbb{R}^{n \times p}$  is the design matrix,  $\boldsymbol{\beta} \in \mathbb{R}^p$  is the vector of regression coefficients, and  $\boldsymbol{\epsilon} \in \mathbb{R}^n$  is the vector of errors. The design matrix contains the observed values of  $p$  predictors, or features, to be included in the regression. For any given integer  $k < p$ , the best subset selection problem amounts to minimizing the regression error using at most  $k$  features among the  $p$  available ones. In the traditional least squares formulation the problem can be written as

$$\begin{aligned} \min_{\boldsymbol{\beta}} \frac{1}{n} \|\mathbf{Y} - \mathbf{X}\boldsymbol{\beta}\|_2^2 \\ \|\boldsymbol{\beta}\|_0 \leq k \end{aligned} \tag{2}$$

where the subset size is restricted to at most  $k$  features through the  $L_0$  constraint  $\|\boldsymbol{\beta}\|_0 = \sum_{i=1}^p I(\beta_i \neq 0) \leq k$ . As pointed out in [Bertsimas et al., 2016], this can be reformulated as a MIQP of the form described in (1) by introducing a vector of binary variables  $\mathbf{z} \in \{0, 1\}^p$  with the following interpretation: if  $z_j = 1$  in the solution, then feature  $j$  is selected, else it is not. The problem then becomes

$$\begin{aligned} \min_{\boldsymbol{\beta}, \mathbf{z}} \frac{1}{n} \|\mathbf{Y} - \mathbf{X}\boldsymbol{\beta}\|_2^2 \\ -\mathcal{M}z_j \leq \beta_j \leq \mathcal{M}z_j & \quad j = 1, \dots, p \\ \sum_{j=1}^p z_j \leq k \\ \beta_j \in \mathbb{R}, \quad z_j \in \{0, 1\} & \quad j = 1, \dots, p \end{aligned} \tag{3}$$

The two parameters  $\mathcal{M}$  and  $k$  play very important roles. Constraining each  $\beta_j \neq 0$  to be within  $[-\mathcal{M}; \mathcal{M}]$  is referred to as the "bigM" trick, and the proper choice of  $\mathcal{M}$  is an art. A sufficiently large  $\mathcal{M}$  guarantees that solutions to (3) are also solutions to (2), but an excessively large one can affect solvability of the problem – mainly for numerical reasons. Using separate bounds  $\mathcal{M} = (\mathcal{M}_1, \dots, \mathcal{M}_p)'$  for each coefficient can increase flexibility in the estimation of  $\boldsymbol{\beta}$ .

[Bertsimas et al., 2016] provide a few options for selecting  $\mathcal{M}$ , as well as a clever formulation that does not require its *a priori* choice. In our implementation we use separate and fairly wide bounds, setting  $\mathcal{M}_j = c|\hat{\beta}_{j, OLS}|$  where  $\hat{\boldsymbol{\beta}}_{OLS}$  are the Ordinary Least Squares (OLS) estimates and  $c$  is some scaling constant (e.g.,  $c = 5$  for our numerical results in Section 4). This choice is based on the assumption that OLS estimates provide a reasonable idea of the magnitude of the true underlying coefficients. Of course, OLS may overestimate the coefficients of non-relevant features and underestimate those of relevant ones – but it provides information on the role of each feature in the regression and, even when inflating by  $c$ , does not seem to lead to solvability issues. The parameter  $k$  has a less technical and rather crucial role for guaranteeing accurate feature selection. It bounds the size of the subset in (3), directly controlling sparsity. If  $k$  is too small, we miss

important signals; if it is too large, we overfit the regression. For large  $p$ , choosing  $k$  by standard tuning methods such as 10-fold cross-validation across its entire range  $\{1, \dots, p\}$  is computationally very demanding, if not prohibitive – even with state-of-the-art solvers. This issue can be mitigated restricting the range of  $k$  at the outset through assumptions. For instance, one may assume that the regression is very sparse and explore only  $k \in \{0, \dots, 10\}$  even though  $p = 100$ , or 1,000 – or more. In many applications though this may not be appropriate. In this regard, we propose specialized search methods that assess the entire range of  $k$ , but maintain computational viability by evaluating only a small portion of its values (see Section 3).

### 2.3 Feature Selection with the LASSO

LASSO regression is a regularization method commonly used for feature selection due to its impressive computational speed and ability to induce shrinkage and fit parameters simultaneously. Similar to (2), LASSO can be expressed as

$$\begin{aligned} \min_{\beta} \frac{1}{n} \|\mathbf{Y} - X\beta\|_2^2 \\ \|\beta\|_1 \leq \lambda. \end{aligned} \tag{4}$$

The key difference between the MIP and LASSO formulations is the choice of penalization term, i.e. the constraint placed on the  $\beta$  coefficients. While MIP uses the  $L_0$  norm, placing a bound  $k$  on the size of the subset (the number of selected features), LASSO uses the  $L_1$  norm, placing a bound  $\lambda$  on the size of coefficient vector. Thus, LASSO does not explicitly solve best subset selection and does not directly control sparsity. Its formulation expresses a simpler optimization problem, having only continuous variables and convex constraints. Many fast algorithms have been proposed for solving LASSO; the most commonly used is a variation of coordinate descent from [Friedman et al., 2010] (a very efficient implementation of LASSO is provided in the `glmnet` R-package). LASSO solution quality, likewise MIP, depends on the choice of its tuning parameter  $\lambda$ . But computational speed makes this straightforward: one generates a fine grid of  $\lambda$  values ranging from maximal to minimal shrinkage (all coefficients are forced to 0 on one extreme, and allowed to take their OLS values on the other). On each grid value one then computes, e.g., a 10-fold cross-validation error, and selects the one minimizing such error. Another choice, which induces more shrinkage and is known as *parsimonious* LASSO, is the largest  $\lambda$  with cross-validation error within one standard deviation from the minimum.

Overall, notwithstanding the efficient tuning made possible by computational speed, LASSO is known for producing solutions with a high number of false positives. In fact, [Tibshirani, 2011] recommended it as a *screen* (instead of a selection procedure), because under certain conditions it achieves the sure screening property. In contrast, the MIP approach has been shown to produce sparser solutions, with fewer false positives – though they may not necessarily have higher prediction accuracy when compared to LASSO.

## 3 Our Proposals

Here we present our novel proposals: two modified bisection procedures for searching across the whole range of  $k$  – but evaluating only a small portion of its values (Section 3.1), strategies for bounds and warm starts (Section 3.2), and an integrated cross-validation scheme (Section 3.3). Our numerical studies (Section 4) show that these proposals lead to a substantial reduction in computational burden, rendering the MIP approach viable in realistic applications. In Section 3.4 we introduce whitening, a pre-processing step which can further increase performance of the MIP approach.

### 3.1 Modified Bisection Procedures

Let  $k_0$  be the true and *unknown* number of features that affect the response and should be retained. For their selection to be effective, an appropriate value for the bound, i.e. an estimate of  $k_0$ , must be obtained from the data. This tuning can be implemented evaluating out-of-sample regression performance via  $v$ -fold cross-validation, and comparing it across all  $k$  values from 1 to  $p$ . For example, the black curve in Figure 1 shows 10-fold cross-validation Mean Squared Error (CVMSE) obtained solving MIQPs at  $k = 1, \dots, p$  on simulated data with  $p = 50$  and  $k_0 = 15$  (see Section 4 for details).

Ideally, the CVMSE curve would decrease (as one adds more relevant features) and then increase (as one overfits adding irrelevant features), identifying an appropriate  $\hat{k}_0$  as a *sweet spot* (minimum). But the *elbow* shape of Figure 1 is typical of many regressions in practice. It still allows us to easily settle on  $\hat{k}_0 = 15$  by parsimony, since the benefit of adding more features is evidently negligible. The problem with employing this strategy when solving MIQPs is the computational burden of

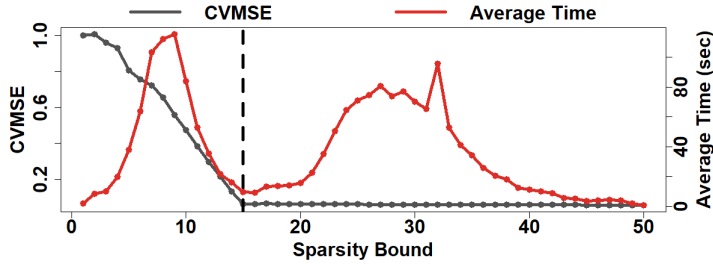


Figure 1: Cross-validation Mean Squared Error (CVMSE) and average computing time (over the 10 folds) across all values of  $k$ , for a simulation scenario with  $p = 50$  features and  $k_0 = 15$ . The dashed line marks the ideal  $k$  bound.

cross-validating across the whole range of  $k$ . If  $p$  is large, this may be unviable because we need to solve as many as  $v \times p$  MIQPs. For very sparse regressions, say  $k_0 \leq 10$ , it may still be feasible to solve  $v$  MIQPs for  $k = 1, 2, \dots$  until it becomes clear that we are past a sweet spot or an elbow in the CVMSE curve. However, if the regression is not very sparse, or if it is only *proportionally* sparse but  $p$  is very large, this will not ensure computational viability. For instance, if we have  $p = 5000$  and the number of true positives is  $k_0 = 10\%p = 500$ , more than 500 values of  $k$  will be cross-validated and more than  $v \times 500$  MIQPs solved to identify a good estimate of the bound.

If we could count on the CVMSE curve having a distinct sweet spot (a single global minimum and a clear quasi-convex shape) one way to tackle this issue would be to use a *bisection procedure* ([Cormen et al., 2009]). A classical bisection would search the whole range  $\{1, \dots, p\}$  of  $k$ , but evaluate only a small portion of its values – limiting the number of MIQPs to be solved to around  $v \times \frac{\log(p)}{\log(2)}$ . However, this could be rather ineffective in identifying the elbow of a CVMSE curve shaped as in Figure 1. Thus, we have designed two bisection procedures specifically modified for this problem. They are described below, and their remarkable performance and robust behavior is demonstrated in Section 4.1.

**Bisection with Feelers:** The first modified bisection utilizes our expectation on the shape of the CVMSE curve to save on the number of functional evaluations. It also operates iteratively, exploring the neighbours of the current  $\hat{k}_0$  to better understand where we are in the CVMSE curve. We name these explorations *feelers*, thus the method is referred to as *bisection with feelers* (BF). We begin with the two end points of the search interval set to  $a = 1$  and  $c = p$ , and split it at its midpoint  $b$  to get  $[a, b]$  and  $[b, c]$ . To decide which of these two intervals to search next, we use

---

**Algorithm 1:** Bisection with Feelers (BF)

---

```

input : Lower bound  $a$  and upper bound  $c$  of the search interval, maximum number of
       iterations  $itermax$ , and thresholds  $\delta$  and  $\epsilon$ 
output: Selected sparsity bound  $\hat{k}_0$ 
1 for  $i = 1$  to  $itermax$  do
2   while  $a \neq b$  do
3     Bisect interval at  $b = \text{floor}(\frac{a+c}{2})$ 
4     Solve for  $M_a$ ,  $M_b$ , and  $M_c$ 
5     Calculate  $RD(a, b)$  and  $RD(b, c)$ 
6     if  $RD(b, c) > \delta$  and  $RD(a, b) > -\delta$  then
7       | Search interval  $[b, c]$  by setting  $a = b$ 
8     else
9       | Search interval  $[a, b]$  by setting  $c = b$ 
10    end
11   end
12   Set  $\hat{k}_0 = c$ 
13   Solve for the two feelers  $M_{\hat{k}_0-1}$  and  $M_{\hat{k}_0+1}$ 
14   Calculate  $RD(\hat{k}_0 - 1, \hat{k}_0)$  and  $RD(\hat{k}_0 + 1, \hat{k}_0)$ 
15   if  $RD(\hat{k}_0 - 1, \hat{k}_0) \geq \epsilon$  or  $RD(\hat{k}_0 + 1, \hat{k}_0) \geq \epsilon$  then
16     | break
17   else
18     | Stuck in the tail, set  $a = 1$ 
19   end
20 end

```

---

relative differences in cross-validation error. In symbols, let  $M_k$  be the set of features selected by the MIQP with a generic  $k$ , and  $f(k)$  the corresponding cross-validation error. We solve for  $M_a$ ,  $M_b$ , and  $M_c$ , and consider

$$RD(a, b) = \frac{f(a) - f(b)}{f(a)|b - a|}, \quad RD(b, c) = \frac{f(b) - f(c)}{f(b)|b - a|}. \quad (5)$$

Given a positive threshold  $\delta$ ,  $RD(b, c) \leq \delta$  is an indication that  $b$  is already past the elbow of the curve; in this case we search  $[a, b]$ . Else, if  $RD(b, c) > \delta$ , we search  $[b, c]$ . However, if  $RD(a, b) > -\delta$  ( $f(b)$  is sufficiently higher than  $f(a)$ ) we have an indication that the curve actually re-increases past a minimum occurring before  $b$ ; candidate values in  $[b, c]$  are subject to overfitting. In this case we search  $[a, b]$  regardless of the value of  $RD(b, c)$ . This continues until the bisection algorithm converges and outputs an estimate  $\hat{k}_0$ . Next, since  $\delta$  clearly affects the bisection output, we send out two *feelers* around the current  $\hat{k}_0$ , computing  $RD(\hat{k}_0 - 1, \hat{k}_0)$  and  $RD(\hat{k}_0, \hat{k}_0 + 1)$ . If these are both smaller than another, stricter threshold  $\epsilon < \delta$ , we have an indication that  $\hat{k}_0$  is already past the elbow of the curve; in this case we restart the algorithm setting  $a = 1$  and  $c = \hat{k}_0$ .

Due to the feelers portion of the BF, the number of evaluations may be higher than  $\frac{\log(p)}{\log(2)}$  – depending on how many times we allow the algorithm to restart and how far past the elbow we are each time. In our numerical studies we typically restart the algorithm at most once; nevertheless, a bound on the number of iterations  $itermax$  is used to avoid excessive computing time. Detailed pseudocode is provided in Algorithm 1.

**Bisection with Randomly Added Variables:** While BF was designed to exploit the shapes generally presented by cross-validation error curves, our second modified bisection saves on the number of function evaluations by comparing the optimal subsets produced by MIQP with perturbed sets containing features selected at random. We call this *bisection with randomly added variables* (BRV). Let  $M_k$  be again the set of features selected by the MIQP with a generic  $k$ , and

$g_{\mathcal{F}}(k)$  the corresponding validation error on fold  $\mathcal{F} = 1, \dots, v$ . Note that this is not the same as the cross-validation error  $f(k)$  used in BF.  $f(k)$  was obtained solving the MIQP on the training data and computing the validation error on the withheld data for each fold of the cross-validation, and then averaging these errors over folds. In BRV, the aim is to compare the set  $M_k$  obtained solving on all the data to another, perturbed set of features. Thus, we fix  $M_k$  and simply refit with OLS (on the training data) and measure validation error (on the withheld data) using the same features across the folds. This provides  $v$  validation errors specific to  $M_k$  that can be used to gauge its quality. Now, let  $M_k^C$  be the complement (the set of  $p - k$  features not contained in  $M_k$ ). At any given  $k$ , we draw from it to generate perturbed sets.

As in BF, we begin with the two end points of the search interval set to  $a = 1$  and  $c = p$ , and split it at its midpoint  $b$  to get  $[a, b]$  and  $[b, c]$ . In BRV, we focus our attention on the mid-point; we solve for  $M_{b-1}$ ,  $M_b$  and  $M_{b+1}$ , obtain  $g_{\mathcal{F}}(b)$  and  $g_{\mathcal{F}}(b+1)$  for  $\mathcal{F} = 1, \dots, v$ , and benchmark these errors as follows. For each fold  $\mathcal{F}$ , let  $g_{\mathcal{F}}^*(b)$  (resp.  $g_{\mathcal{F}}^*(b+1)$ ) be the error that would be obtained if a new feature were added to the set  $M_{b-1}$  (resp.  $M_b$ ) by randomly selecting such a feature from  $M_{b-1}^C$  (resp.  $M_b^C$ ). The construction of an empirical distribution for  $g_{\mathcal{F}}^*(b)$  (resp.  $g_{\mathcal{F}}^*(b+1)$ ) is very simple and economical: for a large enough number  $rep$  of repetitions, one selects a feature at random from the complement set, adds it to the current set, and recomputes the coefficients fixing the variables already selected in  $M_{b-1}$ , resulting in a negligible computational burden. Again for each fold  $\mathcal{F}$ , we can then ask if the error obtained by solving the MIQP with  $b$  (resp.  $b+1$ ) is likely to come from the empirical distribution of  $g_{\mathcal{F}}^*(b)$  (resp.  $g_{\mathcal{F}}^*(b+1)$ ). More precisely, let  $p_b^{\mathcal{F}}$  and  $p_{b+1}^{\mathcal{F}}$  be low quantiles (e.g.,  $\delta_q = 5\%$ ) of the two empirical distributions constructed for  $\mathcal{F}$ . If  $g_{\mathcal{F}}(b) > p_b^{\mathcal{F}}$ , then increasing the size of an optimized set of features from  $b-1$  to  $b$  affords a gain comparable to simply adding a feature at random to the  $b-1$  optimally selected ones. This may be the case for some folds and not others, especially if  $M_{b-1}$  contains many false positives. All together, if  $g_{\mathcal{F}}(b) > p_b^{\mathcal{F}}$  for more than, say,  $\delta_v = 50\%$  of the folds, then we turn our search to  $[a, b-1]$ . On the other hand, if  $g_{\mathcal{F}}(b) \leq p_b^{\mathcal{F}}$  for most folds, then the gain is sizeable, and to decide where to turn our search we consider  $g_{\mathcal{F}}(b+1)$ . If  $g_{\mathcal{F}}(b+1) \leq p_{b+1}^{\mathcal{F}}$  for most folds, then also increasing the size of an optimized set of features from  $b$  to  $b+1$  is better than adding a feature at random to  $b$  optimally selected ones, and this encourages us to search  $[b+1, c]$ . However, if  $g_{\mathcal{F}}(b+1) \geq p_{b+1}^{\mathcal{F}}$  for most folds, then while increasing to  $b$  features results in a sizeable gain, moving any further does not. Thus, we turn our search to  $[a, b]$  – which may allow us to identify an even better bound value to the left of  $b$  (an even sparser solution). This continues until the BRV algorithm converges and outputs an estimate  $\hat{k}_0$ . Detailed pseudocode for this method is provided in Algorithm 2.

### 3.2 LASSO Bounds and Forward Selection-based Warm Starts

Next we address the fact that a single MIQP solution can take very different, and potentially large run times for different values of  $k$ . For example, the red curve in Figure 1 shows average computing times (over cross-validation folds) across values of  $k$  (we solved the MIP at each instance using **Julia** 0.6.1 to interface with **Gurobi** 7.5.1; see Section 4.1). Clearly, some are much higher than others; as to be expected, very small or very large  $k$  values result in faster convergence rates for the optimization solver. Convergence becomes slower as we move inward, though notably it speeds up again around the true  $k_0$ , which is of course unknown in real applications. This behavior illustrates that at least some of the MIQP solution runs required to tune  $k$  are likely to be very costly. What if, in addition to reducing the number of runs (see Section 3.1), we could make the most expensive ones cheaper? Following a well established practice in optimization, we do this generating good starting points for the Branch & Cut procedure utilized when solving MIQPs. Specifically we employ LASSO and forward selection, which are extremely inexpensive to run, to

---

**Algorithm 2:** Bisection with randomly added variables (BRV)

---

```

input : Lower bound  $a$  and upper bound  $c$  of the search interval, number of repetitions
         $rep$ , quantile threshold  $\delta_q$ , and fold threshold  $\delta_v$ 
output: Selected sparsity bound  $\hat{k}_0$ 
1 while  $a \neq b$  do
2   Bisect interval at  $b = \text{floor}(\frac{a+c}{2})$ 
3   Solve for  $M_{b-1}$ ,  $M_b$ , and  $M_{b+1}$ 
4   Calculate  $g_{\mathcal{F}}(b)$ , and  $g_{\mathcal{F}}(b+1)$  for all folds  $\mathcal{F} = 1, \dots, v$ 
5   for  $j = 1$  to  $rep$  do
6     Randomly draw one feature from  $M_{b-1}^C$ , and one feature from  $M_b^C$ 
7     Calculate  $g_{\mathcal{F}}^*(b)$  and  $g_{\mathcal{F}}^*(b+1)$ 
8     Set  $\text{pmse}_b^{\mathcal{F}}[j] = g_{\mathcal{F}}^*(b)$  and  $\text{pmse}_{b+1}^{\mathcal{F}}[j] = g_{\mathcal{F}}^*(b+1)$ 
9   end
10  Set  $p_b^{\mathcal{F}} = q(\text{pmse}_b^{\mathcal{F}}, \delta_q)$  and  $p_{b+1}^{\mathcal{F}} = q(\text{pmse}_{b+1}^{\mathcal{F}}, \delta_q)$  (where  $q()$  is the quantile function)
11  if  $g_{\mathcal{F}}(b) \leq p_b^{\mathcal{F}}$  and  $g_{\mathcal{F}}(b+1) \leq p_{b+1}^{\mathcal{F}}$  for  $\geq \delta_v$  folds then
12    | Search interval  $[b+1, c]$  by setting  $a = b+1$ 
13  else
14    | if  $g_{\mathcal{F}}(b) > p_b^{\mathcal{F}}$  then
15      | | Search interval  $[a, b-1]$  by setting  $c = b-1$ 
16    | else
17      | | Search interval  $[a, b]$  by setting  $c = b$ 
18    | end
19  end
20  Set  $\hat{k}_0 = c$ 
21 end

```

---

generate appropriate *bounds* and *warm starts* for our optimization problem.

When solving the MIQP for a generic  $k$ , termination is established either when a sufficiently small integrality gap is reached (see, e.g., [Schrijver, 1986] or [Chen et al., 2011]), or when a maximum computing time is surpassed. Both rules can be customized in state-of-the-art solvers. In our implementation, we set a gap threshold  $\epsilon_G$ , as customary, but also a reasonable maximum computing time *maxtime*. Suppose that, while searching an interval  $[a, c]$  with one of our modified bisections and solving for an  $M_k$ , we hit such *maxtime*. Then, we run a LASSO on all  $p$  features and obtain the number of features  $k_{LA}$  it would select. Since LASSO tends to retain false positives, we solve for  $M_{k_{LA}-1}$  if  $k_{LA} \leq k$ , and again for  $M_k$  if  $k_{LA} > k$ . Next, we run forward selection for precisely  $k_{LA} - 1$  (or  $k$ ) features and consider the resulting feature selection indicators  $\mathbf{Z}_{FS}$  and coefficient estimates  $\beta_{FS}$ ; this is our warm start. We also run forward selection for  $k_{LA}$  (or  $k+1$ ) features and consider the resulting in-sample mean squared error  $\mathcal{E}_{FS+}$ ; this provides us with a bound for the error. Finally, we run our algorithm using  $\mathbf{Z}_{FS}$  and  $\beta_{FS}$  as our starting point and terminating when the error is within some percentage, say  $p_+$ , of  $\mathcal{E}_{FS+}$ . If  $k_{LA} \leq k$ , we also update the current search interval, setting  $c = k_{LA} - 1$ . If instead  $k_{LA} > k$ , LASSO does not help in adjusting the sparsity bound, but we can still run our algorithm using the forward selection-based warm start and error bound. This greatly curbs computation time in numerical experiments (see Section 4.1) and, notably, generates a solution with at least one fewer feature than the LASSO solution and a smaller or equal error. Detailed pseudocode is provided in Algorithm 3.

---

**Algorithm 3: LASSO Bounds and Forward Selection-based Warm Starts**


---

```

input : Current sparsity bound  $k$ , maximum computing time allowed  $maxtime$ , gap
        threshold  $\epsilon_G$ , and percentage  $p_+$ 
1 Solve for  $M_k$ 
2 if Computing time  $\geq maxtime$  and MIP gap  $\geq \epsilon_G$  then
3   Run LASSO regression on all  $p$  features
4   if  $k_{LA} \leq k$  then
5     Run forward selection to collect  $k_{LA} - 1$  and  $k_{LA}$  features
6     Solve for  $M_{k_{LA}-1}$  using  $\mathbf{Z}_{FS}$  and  $\boldsymbol{\beta}_{FS}$  as starting point
7     Stop optimization algorithm when the objective is within  $p_{F+}$  of  $\mathcal{E}_{FS+}$ 
8     Update current search interval  $[a, c]$  by changing upper bound to  $c = k_{LA} - 1$ 
9   else
10    Run forward selection to collect  $k$  and  $k + 1$  features
11    Solve for  $M_k$  using  $\mathbf{Z}_{FS}$  and  $\boldsymbol{\beta}_{FS}$ 
12    Stop optimization algorithm when objective within  $p_+$  of  $\mathcal{E}_{FS+}$ 
13  end
14  continue search process
15 else
16  continue search process
17 end

```

---

### 3.3 Integrated Cross-Validation

We now describe a procedure that leverages linear constraints in a MIQP to reduce the computational burden of  $v$ -fold cross-validation. For any given fold, solving the MIQP effectively amounts to solving a relaxation of the complete problem, where the constraints associated to the withheld observations are relaxed. Thus, when the focus is switched from one fold to another, it may be very easy to recover the feasibility of the relaxed solution using a dual approach – a step typically integrated in MIP solvers. We call this *integrated cross-validation* (ICV). In symbols, for each fold  $\mathcal{F}$ , we consider a modified version of the optimization problem in (3); namely

$$\begin{aligned}
& \min_{\boldsymbol{\beta}, \mathbf{Z}, \mathbf{e}} \sum_{i=1}^n e_i^2 \\
& - e_i - m_i \leq Y_i - \sum_{j=1}^p \beta_j X_{ij} \leq e_i + m_i \quad i = 1, \dots, n \\
& - \mathcal{M} z_j \leq \beta_j \leq \mathcal{M} z_j \quad j = 1, \dots, p \\
& \sum_{j=1}^p z_j \leq k \\
& \beta_j \in \mathbb{R}, \quad z_j \in \{0, 1\}, \quad j = 1, \dots, p \\
& m_i = \tilde{\mathcal{M}} \times I(i \in \mathcal{F})
\end{aligned} \tag{6}$$

This modification is one of several ways to tell a MIP solver not to consider the constraints associated with some of the observations (the ones withheld in  $\mathcal{F}$ ; this is done through the parameter  $\tilde{\mathcal{M}}$  whose use is similar to that of  $\mathcal{M}$  in Section 2). With this formulation, the first fold solution may be rather expensive, but subsequent ones become very cheap – in effect, the first solution serves as a starting point for the next ones. Relatedly, in our practical experience, the warm start strategy described in Section 3.2 is almost exclusively triggered when pursuing first fold solutions.

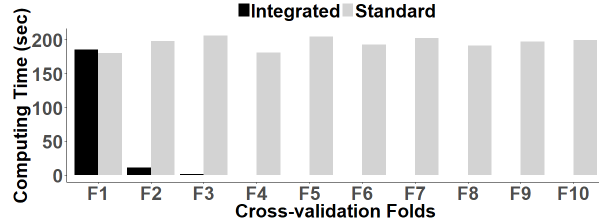


Figure 2: Bar chart of computing times across folds when applying integrated and standard 10-fold cross-validation at  $k = 8$ . The data is simulated from a scenario with  $p = 50$  features and  $k_0 = 15$ .

Notably, the triggering of a warm start in the first fold calculation also provides useful information on the gap. Since  $\mathcal{E}_{FS+}$  is used as a termination threshold on the error, the first fold solution may well have a gap  $\ell_G$  larger than the given  $\epsilon_G$ . However, as pointed out in [Bertsimas et al., 2016] and [Hastie et al., 2017], the solver often reaches an optimal solution, or something very near optimal, earlier than the total solution time may indicate. This is typically due to a weak lower bound on the error that is slow to improve. By using the  $\mathcal{E}_{FS+}$  threshold, we allow the algorithm to stop earlier instead of waiting on improvements to the lower bound.  $\ell_G$  is then used for subsequent folds: in addition to adopting the first fold solution as a starting point, we change the gap threshold to  $\ell_g$  and avoid long computing times from weak lower bounds. The callback feature in modern solvers allows for a simple implementation where the solver periodically checks if the current gap matches or has improved upon that of the first fold. We illustrate the potential benefits of ICV in Figure 2, where we plot computing times across folds for the same simulated data used in Figure 1 at  $k = 8$ . Computing times when using standard cross-validation are provided for comparison. As a final summary, Figure 3 guides the reader through the complete process we employ to tune the sparsity bound  $k$  – utilizing modified bisections, bounds and warm starts, and integrated cross-validation.

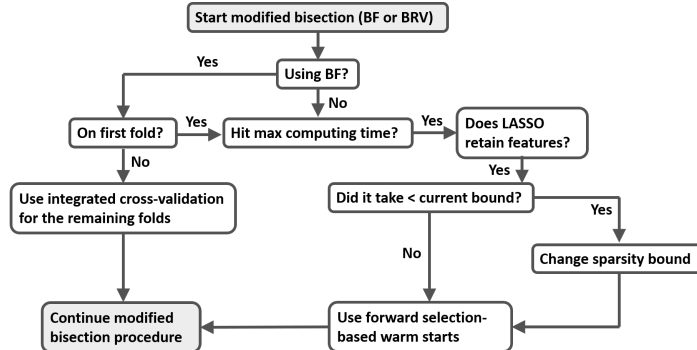


Figure 3: Flowchart illustrating the tuning process for  $k$ . We use one of our modified bisections (BF or BRV), LASSO bound adjustments and forward selection-based warm starts as needed, and integrated cross-validation.

### 3.4 Whitening

Even with procedures that allow us to efficiently and accurately estimate  $\hat{k}_o$  (the true size of the active set), there is no guarantee that the features selected solving for  $M_{\hat{k}_o}$  coincide with the relevant ones, especially in the presence of strong multicollinearity and/or weak signals. In fact, the MIP approach may not fare well in these scenarios. In Figure 4 (and in Figure 1 in the Supplement) we present results obtained solving with the true  $k_o = 10$  on data simulated for a wide range of Signal-to-Noise ratios (SNR; from 0.1 to 10) and highly collinear features. Specifically, we simulated

features following an autoregressive correlation structure with  $\text{corr}(X_\ell, X_j) = \alpha^{|l-j|}$ , and features following a block structure in which  $\text{corr}(X_\ell, X_j) = \rho$  within the sets of relevant and irrelevant features, and  $\text{corr}(X_\ell, X_j) = \omega$  across the two sets (see Section 4 for more details). Figure 4, where  $\alpha = 0.9$ ,  $\rho = 0.5$  and  $\omega = 0.4$ , clearly shows that in the presence of strong collinearity, even using the true  $\hat{k}_o$ , MIQP solutions can lack sensitivity – especially at lower SNR values. By comparing results obtained with and without a data pre-processing step called *whitening*, Figure 4 also shows that MIP recovery can be greatly improved under some circumstances.

In full generality, whitening involves switching from the original  $n \times p$  data matrix  $X$  to a new  $n \times p$  data matrix  $Z = XW$ , where  $W$  (the whitening  $p \times p$  matrix) is chosen so that the transformed features are uncorrelated. For our purposes we use  $W = \hat{\Sigma}^{-1/2}$ , the sample covariance matrix. This is known as ZCA whitening, or ZCA-Mahalanobis whitening, and has the property of minimizing the distance between the original and whitened features; see [Kessy et al., 2018]. The MIP approach can then be applied to select features among the latter and, provided the minimized distance between  $X$  and  $Z$  is small enough, to translate this selection back to the original features. In Figure 4, this allows us to reach almost 100% true positive rate at SNR values  $\geq 0.75$ .

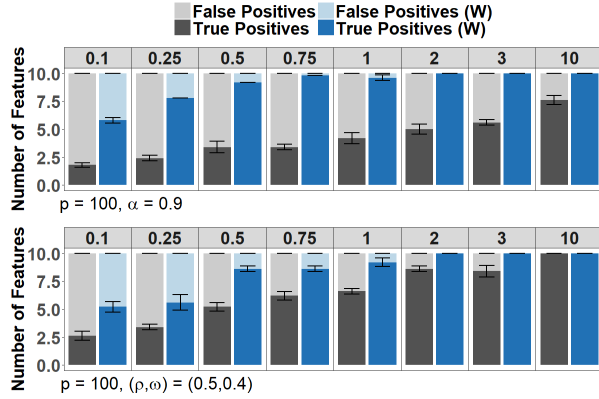


Figure 4: Breakdown in average numbers of true and false positives (with error bars at  $+/ - 1SD$ ) selected solving MIQPs across a range of SNR values (displayed along the top  $x$ -axis). The data are simulated from scenarios with  $p = 100$ ,  $k_0 = 10$ , and highly correlated features with an autoregressive structure (top panel,  $\alpha = 0.9$ ) and a block structure (bottom panel,  $(\rho, \omega) = (0.5, 0.4)$ ). Results are presented before (gray) and after (blue) whitening of the data.

An additional benefit of ZCA whitening is the effect it has on our cross-validation error curves. Figure 5 shows CVMSE over the  $k$  range (1 to  $p = 100$ ) before and after whitening. The data here is simulated with  $k_0 = 10$ ,  $\text{SNR} = 1$ , and features autoregressively correlated with  $\alpha = 0.9$ . Using  $\mathbf{X}$ , noise makes it very difficult to identify an appropriate sparsity bound; simply selecting the minimum would lead to an excessively sparse solution. Using  $\mathbf{Z}$  produces a more distinct "elbow" behavior, so we can get reasonably close to the true  $k_0$ . Interestingly, approaches in the LASSO family do not appear to benefit from whitening as much as the MIP approach. In fact they can be negatively affected by whitening, perhaps because they seem to be prone to specificity rather than sensitivity issues – as mentioned in Section 2.3. We will discuss this in more detail when presenting our numerical results in Section 4.

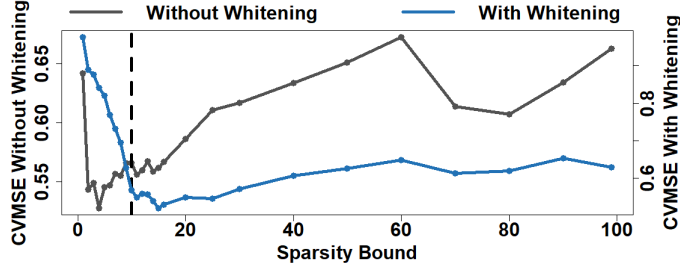


Figure 5: Cross-validation error curves computed with and without whitening (blue and gray respectively). The data are simulated from a scenario with  $p = 100$ ,  $k_0 = 10$  (dashed vertical line), SNR = 1, and highly correlated features with an autoregressive structure ( $\alpha = 0.9$ ).

## 4 Numerical Studies

Here we assess performance of the MIP implemented with our modified bisections, bounds and warm starts strategy, and integrated cross validation. We do this in comparison to LASSO-type methods on both simulated and real data.

### 4.1 Simulation Study

We conduct an extensive simulation study comprising a variety of scenarios defined in terms of problem size  $p$ , sparsity level (the number  $k_0$  of active features), signal patterns (the type of  $\beta$  coefficients), signal to noise ratio (SNR), and the nature and strength of linear association among features. Our enhanced implementation of the MIP approach is compared to LASSO-type methods based on several performance metrics, including computational burden.

We generate the  $n$  rows of the data matrix  $X$  independently from a  $p$ -variate Gaussian distribution. Without loss of generality, we take  $N_p(\mathbf{0}, R)$  – where, in addition to having mean 0, all components have variance  $r_{j,j} = 1$ . Thus, instead of a covariance we specify a  $p \times p$  correlation matrix. We consider two different regimes. The first is an *autoregressive structure*, where  $r_{\ell,j} = \alpha^{|\ell-j|}$  for  $\ell \neq j$ . Here each feature is strongly associated with a few neighboring ones – and only weakly or almost not at all to features further away. If we list the active features as the first  $k_0$ , followed by the  $p - k_0$  inactive ones, potential confounding across the former and the latter occurs for those “within a certain radius” of the boundary at  $k_0$  – depending on the size of  $\alpha \in [0, 1]$ . The second regime, which we call a *block structure*, is one where all active features are pair-wise correlated at level  $r_{\ell,j} = \rho$ ,  $\ell, j \in A$ ,  $\ell \neq j$ , all inactive features are too,  $r_{\ell,j} = \rho$ ,  $\ell, j \in A^C$ ,  $\ell \neq j$ , and across the two sets one also has pair-wise correlations at level  $r_{\ell,j} = \omega$ ,  $\ell \in A, j \in A^C$ . Here the sizes of  $\rho \in [0, 1]$  and  $\omega \in [0, 1]$  control, respectively, the degree of potential confounding among active features, and between active and inactive ones. Notably, each active feature has the same strength of association with *all* inactive features ( $\omega$ ).

The two correlation structures, with appropriately high parameter values, can both represent strong collinearity. However, they are very different and proxy different types of real data settings. This can be appreciated in terms of eigenvalue decay. For example, considering  $\alpha = 0.9$  and  $(\rho, \omega) = (0.5, 0.4)$  in simulations with  $p = 100$  and  $k_0 = 10$ , Figure 6 shows the percentage of variance explained by the first 10 eigenvalues. The autoregressive structure has a much steadier decay compared to the block structure – which has a very dominant first component followed by a sharp drop. The autoregressive structure though also has, in a way, a lower intrinsic dimensionality; its first 10 eigenvalues capture around 98% of the overall variability, while the first 10 eigenvalues

of the block structure only reach 37%. In our experiments we investigated both structures with varying parameter values. Due to space limitations, results below refer to the block structure – but all others are reported in the Supplement.

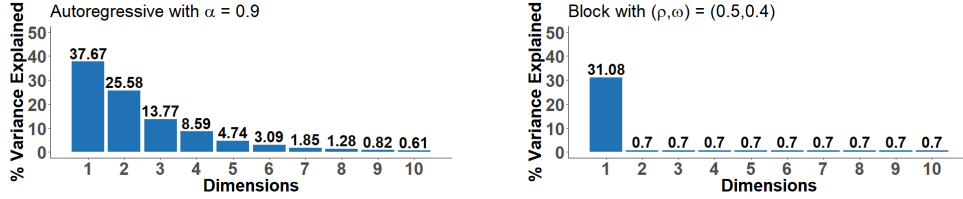


Figure 6: Scree plots illustrating eigenvalue decay in the autoregressive and block correlation structures.

The response is generated through a linear relationship,  $\mathbf{Y} = \mathbf{X}\boldsymbol{\beta} + \boldsymbol{\epsilon}$  where  $\epsilon_i \sim N_p(0, \theta^2 I)$ . Values of  $\theta$  are used to create scenarios with varying SNR, defined as  $\text{SNR} = \frac{\text{var}(\mathbf{X}\boldsymbol{\beta})}{\theta^2}$ . A summary detailing all parameter settings is given in Table 1. To assist with interpretation of the SNR values, we include corresponding regression  $R^2$  values (averaged across simulation runs in each setting). A "realistic" signal to noise ratio may vary depending on scientific fields and class of problems of interest. In recent literature, the MIP approach was shown to perform extremely well (and with a relatively handleable computational cost) in scenarios with very high SNRs ([Bertsimas and Van Parys, 2017]). Conversely, the MIP approach was shown to perform worse than procedures in the LASSO family in scenarios with very low SNRs ([Hastie et al., 2017]). Both extremes may characterize a limited number of real applications. In our experiments we explore a range of SNR values from 0.1 to 10, corresponding to  $R^2$  values from  $\approx 1\%$  to  $\approx 90\%$ . Results below refer to  $\text{SNR} = 0.1, 0.75, 1, 10$  (results for more SNR values are reported in the Supplement).

Table 1: Summary of parameter settings used in the simulation study

Parameter	Values
$n$	500
$p$	100, 1000
$k_0$	10
$(\rho, \omega)$ (BLOCK)	$*(0.5, 0.1)$ , $*(0.5, 0.3)$ , $(0.5, 0.4)$
$\alpha$ (AUTOREG)	$*0.8$ , $0.9$
$\boldsymbol{\beta}$	$(1, 1, 1, 1, 1, 1, 1, 1, 1, 0, \dots, 0)^T$ , $***(10, 10, 10, 10, 10, 10, 10, 10, 5, 5, 5, 0, \dots, 0)^T$
SNR	0.1, $***0.25$ , $***0.50$ , 0.75, 1, $***2$ , $***3$ , 10
$\approx R^2$	0.08, 0.18, 0.32, 0.45, <b>0.51</b> , 0.67, 0.75, 0.91
Replications	5

Asterisks: results in the Supplement. \*\*: 7 stronger and 3 weaker active signals ( $\beta_j = 10$  and 5).

We compare an appropriately tuned MIP, implemented with bisection with feelers (BF) or bisection with randomly selected variables (BRV), the bound and warm start strategy, and integrated 10-fold cross-validation, to: (i) standard LASSO regression tuned by 10-fold cross validation, with the minimizing or the parsimonious choice of  $\lambda$  (LMN and LSD, respectively; see Section 2.3); (ii) the relaxed LASSO of [Hastie et al., 2017] tuned by 10-fold cross validation, with the minimizing choice of  $\lambda$  (RL); (iii) standard forward selection tuned by 10-fold cross validation, with the minimizing choice of subset size (FS). For LMN, LSD, RL and FS we used the R package `bestsubset`

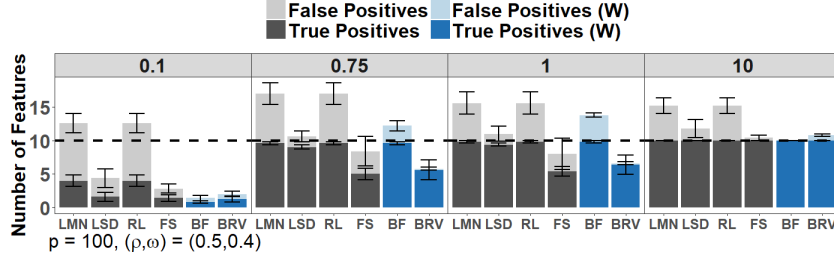
from [Hastie et al., 2017]. For our BF and BRV we used **Julia** 0.6.1, a high-performance dynamic programming language, to interface with the MIP optimization solver **Gurobi** 7.5.1. For our computing time limit, we allowed 10 minutes for scenarios with  $p = 100$ , and 20 minutes for scenarios with  $p = 1000$  (see below). All simulations were performed on the Pennsylvania State Universitys Institute for CyberScience Advanced CyberInfrastructure (ICS-ACI) using the basic memory option on the ACI-B cluster with an Intel Xeon 24 core processor at 2.2 GHz and 128 GB of Ram. The multi-thread option in **Gurobi** was limited to a maximum of 5 threads for consistency across settings. Code for our procedures (written in **Julia**) and for data generation (written in **R**) is available on request – a package for general use is forthcoming. Each simulation scenario is run 5 independent times. As performance metrics, we consider the average number of true positives, which measures *sensitivity*, and the average number of false positives, which measures (lack of) *specificity*. We also consider the average mean squared error computed on separately drawn validation data for each scenario and simulation, which measures *prediction accuracy*. Finally, we consider *accuracy in estimation* of  $\beta$  – partitioned into variance and squared bias. Below we report performance metrics with/without whitening of the data depending on whether it helps/hurts each procedure; in the scenarios considered BF and BVR perform better with whitening, while LMN, LSD, RL and FS perform better on unwhitened data.

#### 4.1.1 Scenarios with $p = 100$

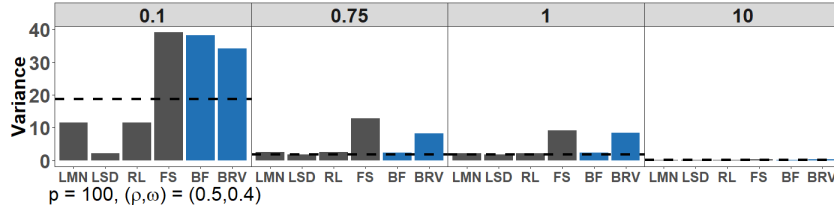
In these scenarios the dimension  $p = 100$  is one fifth of the sample size  $n = 500$ , and the number of active features is  $k_0 = 10$ . Figure 7 summarizes results for the block correlation structure with  $(\rho, \omega) = (0.5, 0.4)$  and SNRs around 0.1, 0.75, 1, and 10. Similar plots are provided in the Supplement for all SNR values and both correlation structures.

In Figure 7(a) we see that all procedures suffer when the SNR is very low – capturing a small number of true positives. Note in particular that an SNR of 0.1 is not low enough to induce superior performance for the LASSO family methods (see [Hastie et al., 2017]) – at least in this high collinearity setting. LMN and RL do select about 10 features (the right number), but not all the selected features are in fact active. The lack of specificity of these procedures does not improve even at higher SNRs. MIP with BF captures all active features at  $\text{SNR} \geq 0.75$ , as do methods in the LASSO family – but unlike the latter it is very specific. FS and MIP with BRV catch up more slowly, but they too capture all active features and are nearly perfectly specific at  $\text{SNR}=10$ .

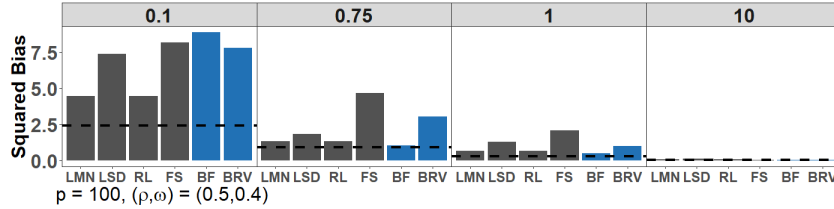
Remarkably, but perhaps not surprisingly given the strong collinearity, these differences in sensitivity and specificity do not translate in substantial differences in prediction accuracy: Figure 7(b) shows that all procedures perform comparably, and better as the SNR increases. However, looking at bias and variance of  $\hat{\beta}$  in Figure 7(c) and (d), respectively, we do again find differences. At an SNR of 0.1, the empirical squared bias of all procedures is significantly worse than that of the OLS estimator fit using only the active features. As to be expected, the overly sparse solutions produced by MIP with BF and BRV, but also by FS and LSD, have larger bias than those of the less specific solutions produced by LMN and RL. Notably though, for mid SNR values, MIP with BF nearly matches the optimal OLS fit, and FS is the most biased at an SNR of 10 all methods have similar and negligible bias. In terms of empirical variance, at low SNRs methods in the LASSO family naturally outperform OLS solutions, as well as FS and the two MIP implementations. However, MIP with BF becomes competitive already at  $\text{SNR} = 0.75$ , and all procedures show similar and very small variance at  $\text{SNR} = 10$ . The poorer estimation performance of MIP with BRV is not surprising, given that it tends to produce sparser solutions (while still maintaining similar prediction error) relative to other procedures. This induces larger differences with the true coefficient values (1 vs 0). In contrast, though methods in the LASSO family lack specificity, the coefficient



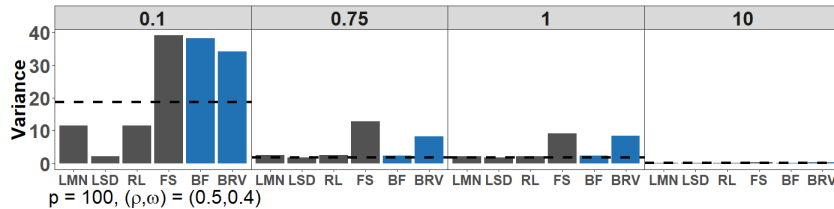
(a) Average numbers of true and false positives over simulation replicates (error bars at  $+/- 1SD$ ). Dotted line at the true number.



(b) Average validation Mean Squared Error over simulation replicates (error bars at  $+/- 1SD$ ). Dotted line: error produced by an OLS fit on the relevant features.



(c) Squared bias of  $\hat{\beta}$  over simulation replicates. Dotted line: squared bias produced by an OLS fit on the relevant features.



(d) Variance of  $\hat{\beta}$  over simulation replicates. Dotted line: variance produced by an OLS fit on the relevant features.

Figure 7: Summary results in scenarios with  $p = 100$ ,  $k_0 = 10$ , various SNR values, and block correlation structure with  $(\rho, \omega) = (0.5, 0.4)$ . Blue=with, gray=without data whitening (depending on the procedure).

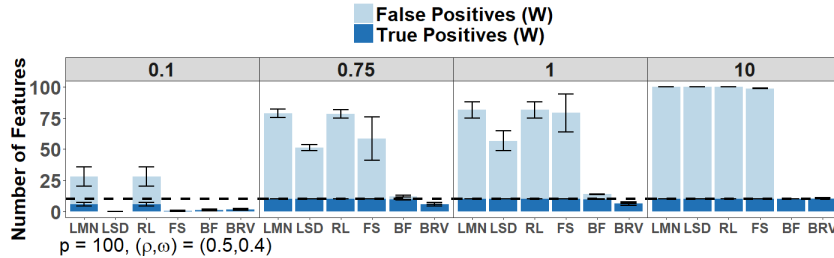
estimates of irrelevant features are likely small and thus induce less of a deterioration in estimation performance.

In Figure 8, we show results when all procedures are applied to whitened data. The SNR reported are again 0.1, 0.75, 1, 10, but similar plots for the complete range of signal strengths are provided in Figure 2 of the Supplement. Figure 8(a) shows how the lack of specificity of methods in the LASSO family becomes rather extreme when they are applied to whitened data. FS, whose specificity is good on the original data, also deteriorates massively under whitening. Figures 8(a) and (b) give some insight on why whitening affects LASSO and MIP procedures so differently. It is clear that, under whitening, the LASSO CVMSE curves give very little indication of where the optimal  $\lambda$  may occur. As the SNR increases, the  $\lambda$  minimizing the error (marked by a circle) gets further and further away from the  $\lambda$  inducing the right level of sparsity (i.e. corresponding to a  $k$  of approximately 10; marked by a triangle). For very weak signals (SNR= 0.1) the two  $\lambda$ 's are close, but Figure 8(a) indicates that this still corresponds to a solution containing many false positives. In contrast, the CVMSE curves for MIP indicate the right level of sparsity much more clearly as the SNR increases. The CVMSE curves shown here were generated by solving the MIP on 10 folds across an entire grid of  $k$  values ranging from 1 to 100 – without the employment of one of our bisections. We still utilized our bounds and warm start strategy, as well as integrated cross-validation, for better efficiency. The effect of whitening on methods in the LASSO family, as well as on other regularization techniques, certainly warrants further simulation and theoretical explorations – which are beyond the scope of the current article. For subsequent results (below and in the Supplement), LASSO procedures and FS are applied to the original data, and MIP procedures are applied to the whitened ones.

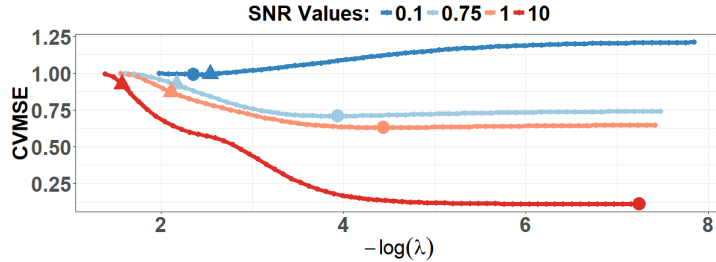
We conclude with a technical note: the performance of MIP with BF shown in Figure 7 for SNR 10 was obtained fixing a more conservative threshold than those used at lower SNR values. Of course, how to set the threshold in the algorithm may not be obvious in practice, but a quick run of the LASSO selecting a very large number of features can inexpensively diagnose the need to implement a restrictive BF. However, we stress that MIP with BF does *not* suffer from the same lack of specificity that hinders LASSO at high SNRs. As discussed above, when the SNR increases the true  $k_o$  becomes in fact easier to identify for MIP; it is simply that the BF search may be pushed towards the right tail of the  $k$  range if seemingly large differences in CVMSE are not “ignored” by setting a stricter threshold. In Figure 8(c), the “elbow” at 10 is clearly denoted when SNR= 10, but the strong signal leads to distinct drops in the CVMSE also at large  $k$  values. Here, a more restrictive threshold easily improves solution quality. In contrast, using a more conservative tuning for LASSO (e.g., the parsimonious LSD), still fails to increase specificity.

#### 4.1.2 Scenarios with $p = 1000$

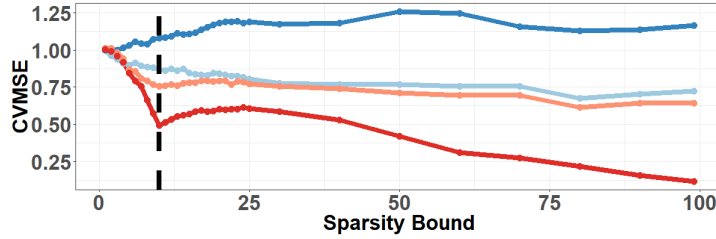
In these scenarios the dimension  $p = 1000$  is twice the sample size  $n = 500$ ; that is, the problem is undersampled. Figure 9 summarizes again results for the block correlation structure with  $(\rho, \omega) = (0.5, 0.4)$  and SNRs 0.1, 0.75, 1 and 10 (complete results are provided in the Supplement). In comparison to the  $p = 100$  scenarios, the MIP procedures have a slightly worse performance. MIP with BF, which was very specific at all SNR values and very sensitive for  $\text{SNR} \geq 0.75$ , retains its specificity but, with  $p = 1000$ , identifies all 10 active features only at  $\text{SNR} = 10$ . MIP with BRV, which produced false positives at low SNR and caught up more slowly than MIP with BF in terms of sensitivity, appears to produce false positives also at higher SNRs – it still does at  $\text{SNR} = 10$ , where it also identifies all 10 active features though. Of course the deterioration of MIP procedures may be due to undersampling. Interestingly, in scenarios with  $p = 1000$ , FS behaves very similarly to the MIP with BF, and the non-parsimonious LASSO procedures LMN and RL



(a) Average number of true and false positives over simulation replicates (error bars at  $\pm 1SD$ ). Data whitened in all procedures



(b) LASSO cross-validation curves under whitening. Triangles mark  $\lambda$  values corresponding to feature subsets of size closest to the true  $k_o$ , and circles those minimizing the cross-validation error.



(c) MIP cross-validation curves under whitening. The vertical dotted line marks the true  $k_o$ .

Figure 8: Summary results for LASSO regression and MIP applied to whitened data. Scenarios with  $p = 100$ ,  $k_o = 10$ , various SNR values, and block correlation structure with  $(\rho, \omega) = (0.5, 0.4)$ .

appear to have higher false positive rates also at low and intermediate SNRs – this, too, could be due to undersampling.

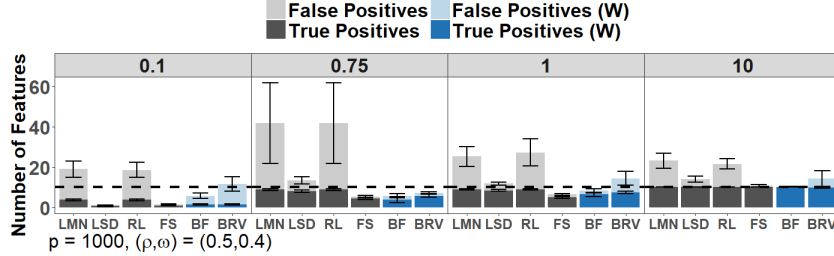
In terms of prediction accuracy, all procedures perform again comparably and better as the SNR increases. In terms of estimation performance, both squared bias and variance of  $\hat{\beta}$  are higher overall in comparison to the  $p = 100$  scenarios. They are also, again, higher for MIP procedures at low SNRs. Notably, MIP with BF does not improve as quickly as when  $p = 100$  and requires higher signal strengths. These behaviors are likely the combined outcome of the overly sparse solutions produced by MIP procedures, and a generally lower accuracy when  $p = 1000$ . Recall that, when  $p = 100$ , even overly sparse solutions produced by MIP with BF and MIP with BRV did comprise only active features. When  $p = 1000$  however, MIP procedures still struggle to select a few of the true features. At low SNRs. An important factor here may be that the inverse square root of the sample covariance matrix represents a rather poor estimate of the whitening matrix for  $n < p$  (we used a simple Moore-Penrose generalized inverse to implement whitening). More accurate estimation of the whitening matrix may enhance the quality of MIP solutions, and consequently the quality of our sparsity bound tuning. We plan to investigate this in more depth in future work.

#### 4.1.3 Sparser Scenarios with $p = 100$

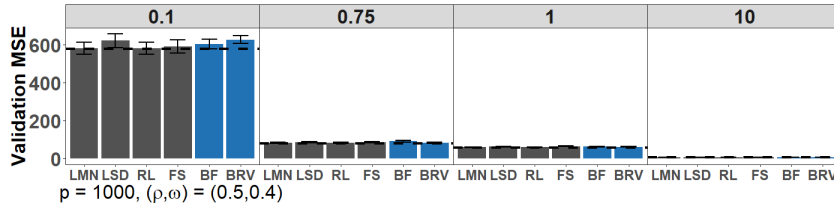
The scenarios with dimensions  $p = 100$  and  $p = 1000$  discussed above all have  $k_o = 10$  active features. Thus, in addition to differing because the latter are undersampled (and the former are not), they also differ in terms of *relative* sparsity: when  $p = 100$ , 10% of the features are active, while this percentage decreases to 1% when  $p = 1000$ . To disentangle the effects of increased sparsity, which may enhance performance, from those of undersampling, which by and large deteriorates it, we consider some additional simulation scenarios where  $p = 100$  (one fifth of the sample size  $n = 500$ , no undersampling) and  $k_0 = 2$  (2% of the features are active). Supplemental Figure 23, like Figures 7 and 9, summarizes results for the block correlation structure with  $(\rho, \omega) = (0.5, 0.4)$  and SNRs around 0.1, 0.75, 1, and 10. In short, the MIP procedures are still more specific than LMS and RL. Surprisingly, only LSD benefits from increased sparsity – even though the  $L_1$  penalty follows the "bet on sparsity" principle ([Friedman et al., 2001]). Overall, the methods that were overly sparse when 10% of the features were active (LSD, FS, and MIP with BRV) now produce the most exact solutions. MIP with BF had to be run again with a restrictive threshold, but this was easy to diagnose as LASSO procedures have very poor specificity even at low SNRs when the data is whitened. Prediction accuracy is comparable for all procedures, much like when 10% of the features were active. In terms of bias and variance of  $\hat{\beta}$ , the parsimonious LSD, which is more specific with higher sparsity, also induces a distinctly larger squared bias. With higher sparsity, the MIP procedures actually outperform all others in terms of bias and have comparable variance at mid to high SNRs.

#### 4.1.4 Computational Burden

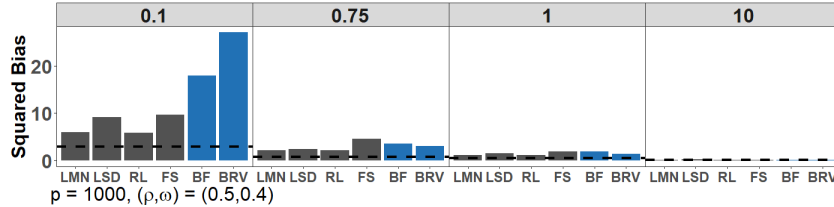
We have shown how our implementation of MIP can be quite effective in terms of active features identification (true and false positives), prediction accuracy, and bias and variance in estimating the coefficients of a linear model. However, a key benefit of our proposals (bisection variants, bounds and warm starts strategy, and integrated cross-validation) is the dramatic reduction of computing time compared to the standard MIP implementation. This renders MIP a viable approach for best subset selection in a broader variety of realistic data scenarios, and with a rigorous tuning of the sparsity bound. Considering the  $p = 100$  scenario with  $k_o = 10$  and SNR= 1, we illustrate this



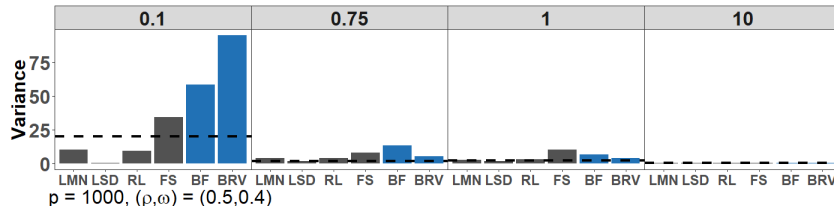
(a) Average numbers of true and false positives over simulation replicates (error bars at  $+/- 1SD$ ). Dotted line at the true number.



(b) Average validation Mean Squared Error over simulation replicates (error bars at  $+/- 1SD$ ). Dotted line: error produced by an OLS fit on the relevant features.



(c) Squared bias of  $\hat{\beta}$  over simulation replicates. Dotted line: squared bias produced by an OLS fit on the relevant features.



(d) Variance of  $\hat{\beta}$  over simulation replicates. Dotted line: variance produced by an OLS fit on the relevant features.

Figure 9: Summary of results in scenarios with  $p = 1000$ ,  $k_0 = 10$ , various SNR values, and block correlation structure  $(\rho, \omega) = (0.5, 0.4)$ . Blue=with, gray=without data whitening (depending on the procedure).

in Figure 10 by comparing computing times between the standard MIP implementation and our implementation – with both BF and BRV (LASSO-type methods are not considered here; they are orders of magnitude faster than MIP implementations).

We allowed all procedures to search across the whole range of possible sparsity bounds ( $k$  from 1 to 100). The left panel shows the total time needed for full tuning (i.e. to identify the optimal sparsity bound). Clearly, the standard MIP implementation required a very large amount of time (almost 4 days) – note this is obtained allowing at most 10 minutes to solve each instance. In comparison, our MIP with BF converged in 3 minutes and our MIP with BRV in 70. The right panel shows the time needed to evaluate each  $k$ . The standard MIP is comparable to our MIP with BF and BRV for only very low or very high  $k$  values – which are, of course, easier to solve. However, it takes up the full allowed time (10 minutes for each of 10 folds, totaling around 100 minutes) for  $k$  values ranging between 10 and 60. Notably, even if we restricted the procedures to search a smaller range, say  $k$  from 1 to 20, the total time for full tuning would still be around 19 hours (1168 minutes) for the standard MIP, as compared to approximately 30 seconds or 30 minutes for our MIP with BF and BRV, respectively.

We note that MIP with BF is much faster than with BRV in this simulation scenario. At the current  $k$ , BF performs 10-fold integrated cross-validation; it solves the program a first time on  $0.9 \times n$  observations (the first fold calculation) and then performs another nine much cheaper runs, each again on  $0.9 \times n$  observations (subsequent folds, see Figure 3). In contrast, BRV is akin to solving the program over  $n$  observations three times; at  $k$ ,  $k - 1$  and  $k + 1$ . If solutions are computationally expensive at and around the current  $k$ , BRV may in fact be more expensive than BF. Of course this is not always the case; the overall cost of BF strongly depends on how cheap are the runs for subsequent folds in our integrated cross-validation. For larger problem sizes, they can still take several minutes, making BRV more competitive.

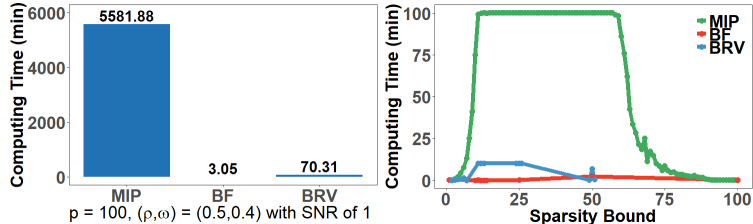


Figure 10: Computing time requirements of the standard MIP (MIP) and the novel MIP with BF (BF) and MIP with BRV (BRV) – using our bisection variants, bounds and warm starts strategy, and integrated cross-validation. The left panel shows total time needed for full tuning of the sparsity bound (in minutes) and the right panel shows the time needed to evaluate each  $k$  in the range from 1 to  $p = 100$ . The true value is  $k_o = 10$ .

#### 4.1.5 Summary

To conclude, we summarize the salient results of our simulation study. In scenarios with highly collinear features:

- The MIP approach strongly benefits from the use of data whitening as a pre-processing step. This not only helps in the selection of relevant features, but also in the tuning of  $k$ .
- MIP with BF and with BRV tend to favor sparser solutions than LMN and RL, with fewer false positives, but also capture more true positives than the parsimonious LSD and FS.

- Unlike the observations in [Hastie et al., 2017], our implementations of MIP are consistently competitive in terms of prediction error – even at SNRs as low as 0.1.
- In problems of relatively small size ( $p = 100$ ), coefficient estimates produced by MIP with BF have very low variance and bias at intermediate and high SNRs. Those by MIP with BRV have higher variation and bias, but are still consistently better than FS.
- In problems of larger size ( $p = 1000$ ), coefficient estimates by LMN, LSD, and RL have the lowest variance and bias.
- LMN, LSD, RL, and FS are strongly unspecific when applied to whitened data – this was documented only in problems of size  $p = 100$  and the behavior of LASSO-type methods under whitening warrants further exploration.
- At high SNRs, MIP with BF is rather sensitive to the choice of threshold in the algorithm. However, the need for a more conservative threshold can be readily diagnosed with a (computationally cheap) LASSO run.
- MIP with BRV is less sensitive to the choice of threshold but can be overly sparse in small problems and include more false positives in larger problems.
- In very sparse problems, the parsimonious LSD, FS, and MIP with BRV are more accurate than the other procedures. MIO with BF and with BRV have low bias and comparable variance for intermediate and high SNRs. Surprisingly, increased sparsity does not improve the specificity of LMN and RL.
- Our implementation of the MIP provides dramatic gains in computational efficiency, making this approach for feature selection feasible in a broader range of applications.

## 4.2 An Application to Diabetes Data

We analyze the diabetes dataset first used in [Efron et al., 2004]. This is a rather low dimensional and well sampled dataset, containing  $n = 442$  diabetes patients and 10 baseline predictors including age, body mass index, average blood pressure, six blood serum measurements, and sex encoded as  $\{0, 1\}$  (although somewhat unorthodox, this matches the treatment in [Efron et al., 2004]). The response is a measure of disease progression one year after the baseline. The number of features considered to model disease progression is actually  $p = 64$ ; in addition to the 10 baseline predictors, these include all their 45 pair-wise interactions (products) and 9 squared terms (the squared term for sex is not included).

We separated the data set into a training set and a test set, with 354 and 88 observations respectively (75-25% breakdown). On the training set, we ran all procedures on both whitened data and data that was simply standardized – i.e. transformed to have mean 0 and variance 1, without eliminating correlations (both LASSO and MIP procedures do need to run on features with equal scaling; see [Friedman et al., 2001]). On the test set, we computed validation Mean Squared Errors, again after whitening or simple standardization. A summary of results is provided in Table 2, which shows also OLS fits of the null and full models (intercept only, intercept and all 64 features). The last column contains the relative decrease in validation MSE between the full model and the models produced by each of the procedures considered. For a generic procedure  $A$  this is defined as

$$\frac{ValMSE_{Full} - ValMSE_A}{ValMSE_{Full}}. \quad (7)$$

Table 2: Summary results for procedures applied to the Diabetes data set.

Procedure	$\hat{k}_0$ (S and W)		ValMSE (S and W)		Relative Decrease (S and W)	
LMN	19	41	0.488	0.631	0.614	0.501
LSD	9	21	0.501	0.550	0.604	0.565
RL	19	41	0.488	0.631	0.614	0.501
FS	16	7	0.523	<b>*0.477</b>	0.586	0.623
BF	2	3	0.513	0.496	0.594	0.608
BRV	2	3	0.513	0.496	0.594	0.608
OLS Null	0		0.989		—	
OLS Full	64		1.265		—	

\*: minimum Validation MSE. **S**: standardization. **W**: whitening.

We observe that MIP procedures generate much sparser solutions, whose prediction accuracy does improve with whitening. MIP with BF and with BRV are also consistent in identifying the same set of features – both with whitening and with simple standardization. For both BF and BRV whitening adds one feature, Lamotrigine (LTG), to the two already selected under standardization, Body Mass Index (BMI) and Mean Arterial Pressure (MAP). Looking at p-values for individual effects, all features are highly significant ( $BMI: 9.25 \times 10^{-14}$ ,  $LTG: 2.67 \times 10^{-13}$  and  $MAP: 2.05 \times 10^{-4}$ ). FS under whitening produces the minimum validation MSE, but with as many as 7 features – the ones identified by BF and BVR, plus 4 more (HDL, TCH, GLU, and the interaction between BMI and MAP). This induces a modest improvement with respect to MIP procedures – in terms of relative decrease in the last column, only 1.5%. p-values for BMI, LTG, MAP and the interaction between BMI and MAP are highly significant. In contrast, p-values for TCH and GLU, albeit selected, are non-significant (0.742 and 0.458, respectively) and HDL is only marginally significant (0.0302). Methods in the LASSO family select a much larger number of features, but again with modest improvements in variance explained in the training set, and with a substantial deterioration in validation MSE. Notably, LMN and the RL of [Hastie et al., 2017] have the same performance – relaxing the LASSO does not appear to improve it on this data.

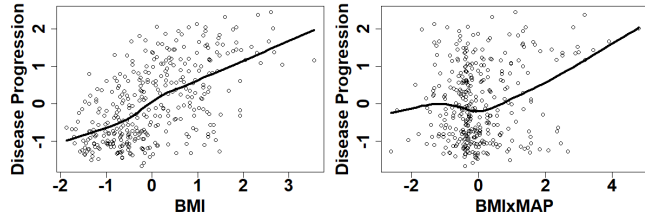


Figure 11: Scatter plots (with fitted curves from the `loess` R function) for Disease Progression against BMI (left) and  $BMI \times MAP$  (right). The interaction term shows a discernible, but weaker and less clear-cut association with the response – which may unfold only at very large values.

The features BMI, MAP and LTG are selected by all procedures considered and have very low p-values in all model fits. They were also included in the best models of [Efron et al., 2004]. The interaction term between BMI and MAP is not selected by MIP with BF and with BRV, but it is selected by all other procedures and significant in the model fits. In fact, its p-value in a 4 feature model comprising BMI, MAP, LTG and  $BMI \times MAP$  is also quite low (0.003) – which leads to the question of whether it ought to have been selected also by the MIP procedures. The right

panel of Figure 11 indeed shows a discernible marginal effect on disease progression, especially at extremely high values of  $\text{BMI} \times \text{MAP}$ . But the improvement in terms of validation MSE is negligible (relative decrease of 0.495 compared to 0.496), as is the one in terms of variance explained in the training set ( $R^2$  of 0.484 compared to 0.472). For comparison, the left panel of Figure 11 shows the much stronger and clearer-cut marginal effect of BMI on disease progression. Of course on a real data problem we have no conclusive way to confirm that we have captured all of the active features, but we have shown that our improved MIP procedures (with modified bisections, bounds and warm starts strategy, and integrated cross validation) can produce sparse, interpretable, and competitive solutions. Importantly, these were also found within a reasonable amount of time. With the relatively small size of  $p = 64$ , the total computing time of MIP with BF was around 13 and 25 minutes for whitened and standardized data, respectively. MIP with BRV was faster on this data set, with computing times around 5 and 8 minutes.

## 5 Concluding Remarks and Future Work

Mixed Integer Optimization for  $L_0$  norm feature selection is receiving much attention due to its foundational appeal, versatility and recent improvements in algorithmic efficiency. However, effectiveness of the MIP approach, like that of regularization methods, depends critically on the selection of a tuning parameter. Pursuing this through cross-validation requires the solution of a very large number of programs – which can still hinder computational viability on problems of realistic size and complexity. We proposed a multi-pronged blueprint for reducing computational burden with modified bisections, bounds and warm starts, and a specialized scheme for cross-validation that takes advantage of the structure of the optimization problem. Importantly, though our proposals were described for linear models, the procedures are very general and could easily be extended to generalized linear models and other classes of statistical models.

Also importantly, the ability to tune effectively and within a feasible timeframe does not fully guarantee the quality of solutions – for MIP as well as other feature selection approaches. Data with strong feature collinearity and/or weak regression signals can deteriorate specificity, sensitivity, prediction or estimation even when the optimization is well tuned (for MIP, when one has a perfect or near-perfect estimate  $\hat{k}_0$  of the number of active features). In our numerical studies the MIP approach substantially benefits from ZCA whitening, a data pre-processing step that de-correlates the features. Whitening is not a new concept, but it too is attracting increasing attention among statisticians. For instance, [Kessy et al., 2018] show how different forms of whitening can benefit different statistical problems. Surprisingly, while our numerical studies suggest that whitening improves recovery of MIP procedures, they do not show a positive effect on LASSO performance. This may be due to the fact that LASSO suffers from poor specificity, not poor sensitivity. The effects of whitening on various features selection approaches (MIP, regularization methods, forward selection, etc.) deserve further investigation. In particular, with regards to MIP procedures, it will be critical to investigate whether and how fast an increase in the distance between original and ZCA whitened features erodes the gains in recovery.

We can envision several other avenues for future work. In our simulations, scenarios with strong signals induced false positives for MIP with BF which were easily prevented using stricter thresholds. This suggests improving our modified bisections with data-driven adaptive thresholding. Moreover, we could incorporate new techniques to generate cuts within the Branch and Bound algorithm and increase efficiency – e.g. a cutting plane method proposed in [Bertsimas and Van Parys, 2017] for sparse ridge regression showed very good performance, in terms of feature selection and computational efficiency, under low to mild feature collinearity and fairly strong signals. Cuts constructed

to exploit problem structure, but not necessarily data structure, are common in Operations Research: knapsack covers, cliques and Gomory cuts are routinely built into commercial solvers (for a survey of potentially useful cutting planes see [Marchand et al., 2002]). While it generally leverages types of MIP formulation (problem structure), the cutting framework is extremely versatile; one can introduce constraints to incorporate *data* structures instead. This was explored in [Bertsimas et al., 2017], where constraints were added to balance specific, competing goals of the modeler – but not to exploit data structures for improving solution quality and computing time.

## References

[Bertsimas et al., 2017] Bertsimas, D., King, A., et al. (2017). Logistic regression: From art to science. *Statistical Science*, 32(3):367–384.

[Bertsimas et al., 2016] Bertsimas, D., King, A., Mazumder, R., et al. (2016). Best subset selection via a modern optimization lens. *The Annals of Statistics*, 44(2):813–852.

[Bertsimas and Van Parys, 2017] Bertsimas, D. and Van Parys, B. (2017). Sparse high-dimensional regression: Exact scalable algorithms and phase transitions. *arXiv preprint arXiv:1709.10029*.

[Chen et al., 2011] Chen, D.-S., Batson, R. G., and Dang, Y. (2011). *Applied Integer Programming: Modeling and Solution*. John Wiley & Sons.

[Cormen et al., 2009] Cormen, T. H., Leiserson, C. E., Rivest, R. L., and Stein, C. (2009). *Introduction to algorithms*. MIT press.

[Efron et al., 2004] Efron, B., Hastie, T., Johnstone, I., Tibshirani, R., et al. (2004). Least angle regression. *The Annals of statistics*, 32(2):407–499.

[Felici et al., 2017] Felici, G., Tripathi, P., Evangelista, D., and Guarracino, M. R. (2017). A mixed integer programming-based global optimization framework for analyzing gene expression data. *Journal of Global Optimization*, 69(3):727–744.

[Friedman et al., 2001] Friedman, J., Hastie, T., and Tibshirani, R. (2001). *The elements of statistical learning*, volume 1. Springer series in statistics New York, NY, USA:.

[Friedman et al., 2010] Friedman, J., Hastie, T., and Tibshirani, R. (2010). Regularization paths for generalized linear models via coordinate descent. *Journal of statistical software*, 33(1):1.

[Hastie et al., 2017] Hastie, T., Tibshirani, R., and Tibshirani, R. J. (2017). Extended comparisons of best subset selection, forward stepwise selection, and the lasso. *arXiv preprint arXiv:1707.08692*.

[Hazimeh and Mazumder, 2018] Hazimeh, H. and Mazumder, R. (2018). Fast best subset selection: Coordinate descent and local combinatorial optimization algorithms. *arXiv preprint arXiv:1803.01454*.

[Kessy et al., 2018] Kessy, A., Lewin, A., and Strimmer, K. (2018). Optimal whitening and decorrelation. *The American Statistician*, pages 1–6.

[Lan and Vucetic, 2013] Lan, L. and Vucetic, S. (2013). Multi-task feature selection in microarray data by binary integer programming. In *BMC proceedings*, volume 7, page S5. BioMed Central.

[Marchand et al., 2002] Marchand, H., Martin, A., Weismantel, R., and Wolsey, L. (2002). Cutting planes in integer and mixed integer programming. *Discrete Applied Mathematics*, 123(1-3):397–446.

[Mazumder et al., 2017] Mazumder, R., Radchenko, P., and Dedieu, A. (2017). Subset selection with shrinkage: Sparse linear modeling when the snr is low. *arXiv preprint arXiv:1708.03288*.

[Meier et al., 2008] Meier, L., Van De Geer, S., and Bühlmann, P. (2008). The group lasso for logistic regression. *Journal of the Royal Statistical Society: Series B (Statistical Methodology)*, 70(1):53–71.

[Miyashiro and Takano, 2015] Miyashiro, R. and Takano, Y. (2015). Mixed integer second-order cone programming formulations for variable selection in linear regression. *European Journal of Operational Research*, 247(3):721–731.

[Schrijver, 1986] Schrijver, A. (1986). *Theory of linear and integer programming*. John Wiley & Sons, Inc. New York, NY, USA.

[Tibshirani, 1996] Tibshirani, R. (1996). Regression shrinkage and selection via the lasso. *Journal of the Royal Statistical Society. Series B (Methodological)*, pages 267–288.

[Tibshirani, 2011] Tibshirani, R. (2011). Regression shrinkage and selection via the lasso: a retrospective. *Journal of the Royal Statistical Society: Series B (Statistical Methodology)*, 73(3):273–282.

[Willis and von Stosch, 2017] Willis, M. J. and von Stosch, M. (2017). L0-constrained regression using mixed integer linear programming. *Chemometrics and Intelligent Laboratory Systems*, 165:29–37.

[Zou and Hastie, 2005] Zou, H. and Hastie, T. (2005). Regularization and variable selection via the elastic net. *Journal of the Royal Statistical Society: Series B (Statistical Methodology)*, 67(2):301–320.